JOURNAL GEOLOGICAL SOCIETY OF INDIA
Vol.66, December 2005, pp.725-740

Plume Generated Mesoproterozoic Mafic-Ultramafic Magmatism in the Chotanagpur Mobile Belt of Eastern Indian Shield Margin

N. C. GHOSE[1+], D. MUKHERJEE[1] and N. CHATTERJEE[2]
[1]Department of Geology, Patna University, Patna - 800 005
[+]Current address: G/608, Raheja Residency, Koramangala, Bangalore - 560 034
[2]Department of Earth, Atmospheric and Planetary Sciences, MIT, Cambridge, Massachusetts 02139
Email: ghosencprof@rediffmail.com

Abstract: The Chotanagpur gneiss-granulite complex (CGGC) – a mobile belt north of the Archaean Singhbhum cratonic nucleus and contiguous orogenic belt with the Singhbhum Proterozoic basin, is a vast tract of high-grade rocks and gneisses with enclaves of granulite and metasedimentary rocks, and intrusive granites of Proterozoic age. Pervasive intrusions of mantle-derived rocks of varied composition ranging from mafic-ultramafic, sodic-ultrapotassic alkaline rocks, massif anorthosite to younger tholeiitic basalts (Rajmahal) and dolerite at different geological periods ranging from Late Paleoproterozoic to Early Tertiary, give evidence of an active mantle in the prolonged history of evolution of this mobile belt. The present study is limited to metamorphosed mafic-ultramafic rocks at the eastern sector of CGGC.

The mafic-ultramafic suite is represented by amphibolite, basic granulite and hornblendite. Compositions of the primary amphibole in these rocks range from hornblende to pargasitic hornblende, and plagioclase from An_{40} to An_{59}. Positive correlation of Mg# between clinopyroxene and hornblende, and clinopyroxene and orthopyroxene, indicating that the Fe-Mg exchange K_D is constant between the ferromagnesian minerals, and the rocks to have attained equilibrium conditions of metamorphism. Calculated post-peak metamorphic equilibrium pressures and temperatures are 3.8-5.4 kb and 643-781°C, similar to conditions in the surrounding country rocks.

Chemically, the metabasic rocks studied are associated with the Bengal anorthosite massif at Saltora and have been grouped into low-Ti and high-Ti tholeiites. The former shows similarity with transitional basalts derived from T-MORB, while the latter is rich in incompatible elements and shows affinity with basalts derived from E-MORB or from recycled mantle fed by subducted oceanic crust. The nepheline normative ultramafic rock is the most depleted in incompatible elements and shows similarity in trace element contents with MORB. All these rocks show variable crustal contamination. Nevertheless, the bulk chemical compositions of the low-Ti rocks preserve evidence of low-pressure fractional crystallisation involving olivine, plagioclase and clinopyroxene. The intra-cratonic Mesoproterozoic bi-modal (tholeiitic-alkaline) magmatism in CGGC is analogous to Phanerozoic magma generation (Rajmahal tholeiites-ultrapotassic mafic-ultramafic intrusions in the Gondwana basins) in a rift setting (Damodar graben / shield margin faults) accompanied with crustal thinning. The trace element geochemistry of mafic-ultramafic rocks gives evidence of plume- generated magmatism in the Eastern Indian Shield margin during Mesoproterozoic time, which is correlatable with the global thermal event in the Precambrian shields.

Keywords: Mafic-ultramafics, Mesoproterozoic, Intracratonic magmatism, Mantle plume, Chotanagpur gneiss-granulite complex, Eastern India.

INTRODUCTION

The Eastern Indian Shield comprises two distinct crustal segments *viz.* Singhbhum Crustal Province (SCP) in the south and Chotanagpur Crustal Province (CCP) in the north (Fig. 1). The SCP comprises an Archaean cratonic nucleus (3.3 Ga, Sharma et al. 1994) and an arcuate belt of volcano-sedimentary assemblages of Singhbhum Proterozoic basin in the north separated by Singhbhum shear zone. The greenschist facies bi-modal basic-ultrabasic (tholeiite-komatiite) association of Dalma Group, developed as a mid-basinal ridge system, is an important landmark in the Singhbhum Proterozoic basin. The CCP is a highland comprising essentially of high-grade gneisses and migmatites containing enclaves of metasediments and mafic and ultramafic rocks, forming the basement of Paleo-Proterozoic age, punctuated by late intrusives of varied compositions. Basic magmatism in both the SCP and CCP played a major role in the crustal evolution of the Eastern Indian Shield.

0016-7622/2005-66-6-725/$ 1.00 © GEOL. SOC. INDIA

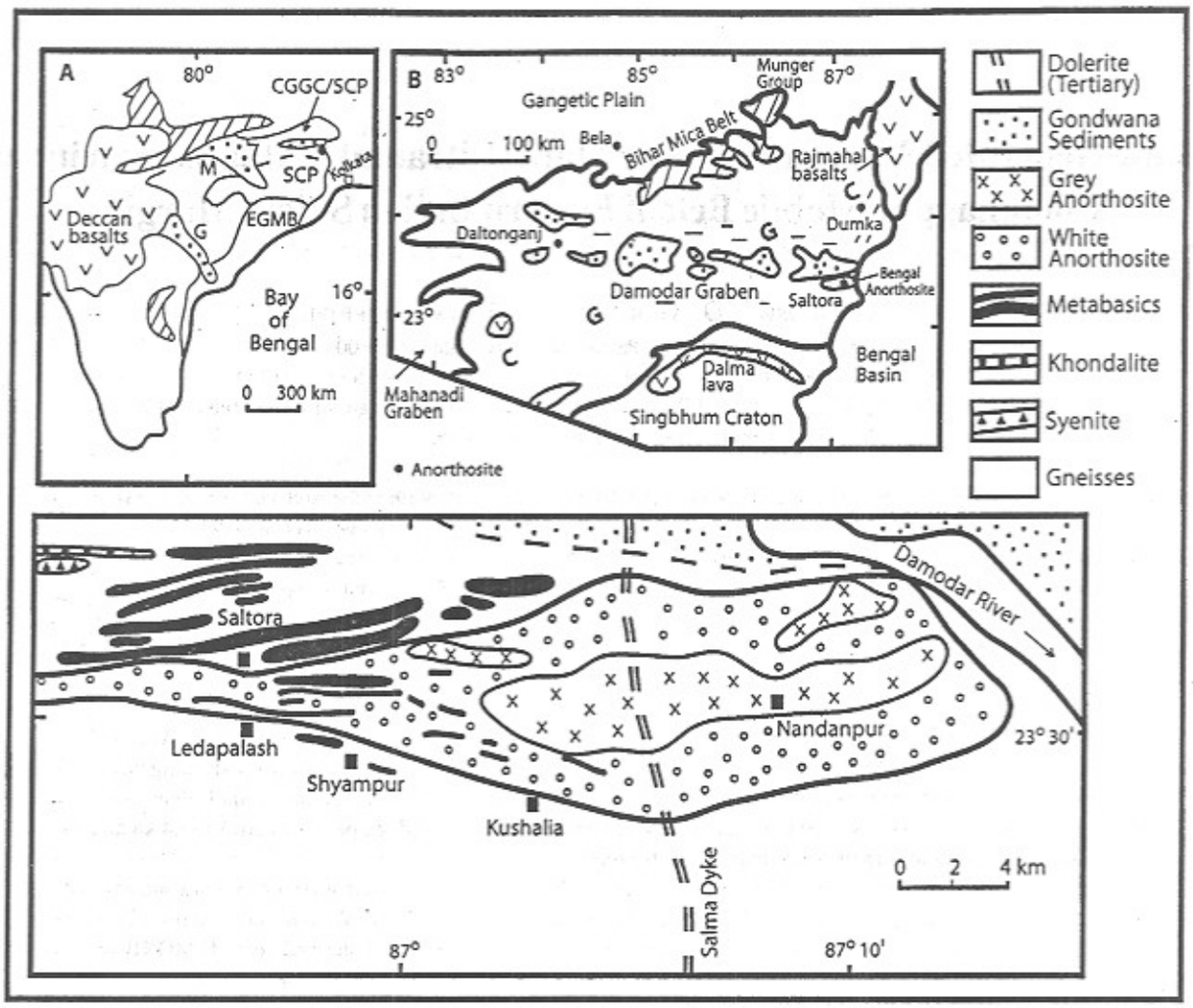

Fig.1. Simplified geological map of Bengal anorthosite associated with metamorphosed mafic-ultramafic rocks in the Chhotanagpur gneissic terrain. Inset (A) Location map of Bengal anorthosite at Saltora (solid circle). EGMB - Eastern Ghats Mobile Belt, SCP - Singhbhum Crustal Province, CGGC - Chotanagpur Gneiss Granulite Complex , CCP- Chotanagpur Crustal Province, D- Damodar graben, dashed line - Singhbhum shear zone, stippled area - Gondwana basins, Mahanadi basin (M), Godavari basin (G), and inclined bar- Proterozoic basins. *Inset* (B) The Chotanagpur gneiss-granulite complex (CGGC).

The easternmost part of CCP tectonically embraces the intersection of two orogenic belts, viz. ENE-WSW to E-W trending Satpura orogenic trend of Chotanagpur plateau and the northeastern extension of Eastern Ghats orogenic trend (NNE-SSW) (Ghose, 1983). These two orogenic trends coincide with two mega-lineaments manifested by basin margin fault of Damodar graben (Gondwana basin) and the Eastern Indian Shield margin fault (Fig. 1). This zone of intersection of two megalineaments, is characterised by diverse types of magmatism ranging in composition from mafic-ultramafic, ultrapotassic / sodic alkaline, granitic and anorthositic rocks belonging to Mid-Proterozoic to Early Tertiary age (Mukherjee and Ghose, 1999). Of these, the basic magmatism and granite plutons are most widespread throughout the Chotanagpur gneiss-granulite complex (CGGC) (Ghose, 1992), designated as 'mobile belt' (Naqvi and Rogers, 1987).

Gravity studies show that a large part of the Chotanagpur plateau is underlain by high density rocks (Verma et al. 1988; Mukhopadhyay, 1987) marked by the presence of gabbroids, ultramafic pockets and swarms of basic sills, largely controlled by second phase of deformation (D_2). These mafic-ultramafic intrusives of varied dimensions, mostly occurring as concordant bodies and now represented by amphibolites, metagabbros, metanorites, metadolerites and metaultramafics, are co-folded with gneisses and

metasediments. Bimodal gabbro/norite-anorthosite magmatism in the CGGC and the younger Proterozoic sub-basins (*viz.* Bihar mica belt or BMB, Gaya-Rajgir and Munger) in the north (Mukherjee and Ghose, 1992; Ghose and Mukherjee, 2000) is contemporaneous with the mafic-ultramafic magmatism. Field relations indicate that the basic magmatism was succeeded by the emplacement of massif anorthosite, granite plutons and pegmatites in order of sequence both in the CGGC as well as in the northern sub-basins. While reviewing the basic magmatism in the Chotanagpur mobile belt, Mahadevan (2002) indicated that they might be older than 1600 Ma.

In the absence of any precise radiometric data on the basic magmatism, the age of early emplacement of the granite at Rajhara, Daltonganj (1741±65 Ma; Ray Barman and Bishui, 1994) and from BMB (1590±30 Ma; Pandey et al. 1986) may be considered as the minimum age, for the mantle-derived mafic-ultramafic intrusives in the Chotanagpur mobile belt (CMB). These granite emplacement events coincide with the global thermal events (1.7-1.6 Ga, Peucat et al. 1999; Oliver and Fanning, 1997; Roy et al. 2002) in the adjoining Precambrian shields of Antarctica, Southwest Australia and Eastern India.

The mafic-ultramafic rock association in close proximity to Bengal anorthosite in CGGC provides an interesting subject for studying the tectono-magmatic history at the Eastern Indian Shield margin. The present study aims to focus the characteristic petrological and chemical features of these metamorphosed mafic and ultramafic intrusives in the high-grade gneiss-migmatite terrain in tracing the tectonic setting of magma generation, their relationship with the mantle composition and probable heat source.

GEOLOGICAL SETTING

The CGGC comprises high-grade metasediments, gneisses, migmatites, khondalite, leptynite, granulite and meta-igneous rocks, which have been intruded by mafic-ultramafic rocks, gabbro-anorthosite, granite, rapakivi granite, syenite, nepheline syenite, lamproite/orangeite, pegmatite, aplite and dolerite, and tholeiitic basalts (Rajmahal Traps) at different geological periods (Mukherjee and Ghose, 1992, 1999; Ghose and Mukherjee, 2000). The gneisses form the country rock and contain numerous enclaves of metasediments, viz. mica schist, sillimanite-biotite-graphite schist, crystalline limestone and dolomite, quartzite, leptynite and granulite. These have been intruded by swarms of basic sills, dykes and plutons now represented by meta-ultramafics, metagabbros, metanorites and amphibolites. The country rocks show a dominant phase of amphibolite facies metamorphism grading into granulite facies. Subsequently, emplacement of granite plutons (dominantly peraluminous) marks a major tectonic event that possibly was responsible in resetting the earlier events (Ghose et al.1973). The mafic-ultramafic intrusives preceded the major granitic activity at 1600 Ma (Pandey et al. 1986) as evident from the occurrence of the former as enclaves within the latter.

The Bengal anorthosite massif emplaced into the CGGC is an E-W trending 40 km long concordant tadpole-shaped body, with a central width of 8 km, covering an area of about 250 km^2 (Fig. 1). Various types of xenoliths entrained within this plutonic mass include metabasics, metasediments and basement gneisses. Among these, the metabasic xenoliths are the most widespread within the massif. These rocks also occur in the surrounding high-grade gneissic country. The imprints of multi-deformational history are well documented in the metasedimentary rocks and gneisses. The inter-relationship of primary flow structure and regional pervasive diastrophic structure at the eastern fold closure (near Nandanpur) suggests *syn- to post-kinematic* status of anorthosite emplacement with respect to D_2-deformation (Mukherjee, 1995). Development of garnet, hornblende and biotite towards the margin of the anorthosite massif suggests crustal contamination and efficacy of volatiles in late crystallisation.

Presence of a large number of sub-parallel E-W trending, discontinuous bands of metabasics both within as well as outside the Bengal anorthosite massif is a remarkable feature. The metabasic rocks are probably not genetically connected to the massif anorthosite (Roy and Saha, 1975; Mukherjee, 1993). The ubiquitous presence of these mantle-derived rocks as a precursor to anorthosite magmatism makes them an interesting subject of studying crust-mantle interaction in the relatively juvenile Mesproterozoic crust of CMB. These metabasics range in thickness from less than a centimetre to several metres, and extend as detached bands often to a few kilometres in length. The metabasic bands on regional scale show greater abundance at the western and southwestern margins of the anorthosite massif. Branching of a single band of metabasic rock, bifurcation of thicker ones and interfingering patterns are common. Long, linear metabasic lenses (e.g. at northeast of Ledapalash) defining macro-banded structures within anorthosite massif show pinch and swell structures. The salient features of the metabasic rocks and their relationship with the anorthosite are as follows:

(i) Irregular patches/pockets of metabasic rocks within the anorthosites,

(ii) Veins and tongues of anorthosite within the metabasics,

Table 1. Petrographic details of the chemically analysed mafic–ultramafic samples in the eastern sector of CMB

Sample No.	B46	C1	B5	B9	B15	B20	C14
Rock Type	**Ultramafic (meta)**	**Low-Ti Metabasic**					**High-Ti Metabasic**
Location	ESE of Shyampur	NNE of Ledapalash (borehole)	NNE of Ledapalash	NNE of Ledapalash	NNE of Ledapalash	West of Shyampur	NNE of Ledapalash (borehole depth of 175.6m)
Mode of occurrence	Within the country rock, outside massif	Within the massif (near surface)	Within the massif	Within the massif	Within the massif	Within the country rock, outside massif	Within the massif (at subsurface level)
Texture	Coarse-grained, vague gneissic fabric	Very fine-grained micro-granular with large porphyroblasts. Retrograde texture	Coarse grained, granular, relict igneous texture	Medium-grained, equigranular, nematoblastic texture	Fine to medium-grained, nematoblastic texture, mineral grains show sieve texture	Medium-grained, equigranular, nematoblastic texture	Medium-grained with larger porphyroblasts, mortar texture and micro-shear planes
Microscopic Structure			Extension (pull apart) cracks filled by amphiboles and opaques. Abundant quartz and some feldspar crushed and granulated				Micro-shear planes filled by secondary minerals like epidote. Parallel arrangements of brown biotite defines a micro-linear / planar feature
Mineral characters	**Hbl** – subhedral to euhedral grains, greenish yellow in colour, **Cpx** – intergrown with Hbl, **Scp** – large grains at grain boundaries of Hbl and Cpx.	**Hbl** – large grains, yellowish green in colour, **Opx** and **Cpx** – small grains around larger Hbl and Plg grains, **Plg** – large grains, both twinned (lamellar) and untwinned, **Qz** – small grains evenly distributed, **Ilm** – abundant small grains	**Hbl** – brownish green in colour, alters to tremolite and chlorite **Plg** – occur both as inclusion within Amp and as discrete grains, the former is untwinned and sericitised, alters to epidote and zoisite, **Qz** – mostly crushed and granulated, some platy, associated with Plg, **Ilm** – abundant small grains	**Hbl** – usually euhedral to subhedral, **Cpx** – shows alteration to tremolite along grain boundaries and cleavage traces, **Opx** – forms a mosaic with Hbl and Cpx , and Plg, **Plg** and **Qz** – large Plg grains associated with small Qz grains at grain boundaries, **Ilm** – abundant small grains	**Hbl** – green in colour, some yellowish-brown secondary amphibole also present. Mafic minerals are more abundant than felsic constituents, **Opx** and **Cpx** – medium sized grains forming a mosaic with larger Hbl grains, **Plg** and **Qz** – large Plg grains associated with small Qz grains at grain boundaries **Ilm** – abundant small grains	**Hbl**, **Opx** and **Cpx** - forming an equigranular mosaic, **Plg** and **Qz** – large Plg grains associated with small Qz grains at grain boundaries, **Ilm** – less abundant than in other	**Hbl** – green in colour, two modes, poikilitic grains and small, prismatic, subhedral to euhedral grains, contains inclusions of Plg, secondary tremolite associated with brown Bt. Alteration of Hbl to green Bt along grain boundary shows release of iron along the cleavage traces. **Bt** – brown in colour, occurring both as inclusion and cross-cut relationship with Hbl, **Plg** – Small granular mostly untwined, few show lamellar twinning, rarely pericline, **Qz** – minor as inclusions within amphibole showing overgrowth of green chlorite. **Ilm** – primary Ilm occurring as skeletal grains, granular secondary magnetite formed as a product of alteration of mafic minerals, **Apt** – abundant small grains

Abbreviations: Hbl – hornblende, Plg – plagioclase, Cpx – clinopyroxene, Opx- orthopyroxene, Qz – quartz, Bt – biotite, Scp – scapolite, Apt – apatite, Ilm – ilmenite

(iii) Interfingering relationship between metabasic and anorthosite, and

(iv) Metabasic rocks occurring both inside and outside the anorthosite massif have identical mineralogical composition.

All these features are not only restricted to surface outcrops but also observed at subsurface levels in drill core samples (Mukherjee, 1995).

PETROGRAPHY AND MINERAL CHEMISTRY

A large number of metabasic rocks such as amphibolites and basic granulite (with or without garnet) showing a wide variation in texture, structure and mineralogy occur in and around the massif anorthosite of Bengal (Sen and Manna, 1976; Bhattacharya and Mukherjee, 1987; Sen and Bhattacharya, 1993; this study). Five of these samples, four occurring inside the massif NNE of Ledapalash and one from the country rock west of Shyampur, are described in detail in this study. In addition, a hornblende-rich ultramafic rock collected from the country rock ESE of Shyampur and a sheared metabasic rock retrieved from a borehole depth of 175.6m NNE of Ledapalash are also studied here in detail (Table 1). Major element compositions of minerals were analysed by wavelength dispersive spectrometry on a JEOL JXA-733 Superprobe at Massachusetts Institute of Technology, Cambridge, U.S.A. The accelerating voltage and beam current used were 15 kV and 10 nA respectively. Typical counting times were 20-40 seconds and 1σ standard deviations of the counts were 0.5-1%. The data were reduced with the CITZAF program (Armstrong, 1995) using the atomic number correction of Duncumb and Reed, Heinrich's tabulation of mass absorption coefficients and the fluorescence correction of Reed. Modal volume percent of minerals were determined through analysis of backscattered electron images collected also with the electron microprobe. Mode of occurrence and petrographic details of the samples in thin sections are summarised in Table 1 and the modal data are presented in Table 2. Mineral compositions are presented in Table 3.

The coarse-grained hornblende-rich ultramafic rock devoid of plagioclase occurs in the country rock at the southern margin of the anorthosite massif. It shows a crude gneissic fabric. It is dominantly composed of subhedral to euhedral grains of primary hornblende (69% by vol.) intergrown with clinopyroxene (19% by vol.). Significant amounts of intergranular scapolite (12% by vol.) occur as large grains. Apatite, sphene, zircon, ilmenite and Fe-sulphides occur as accessory minerals.

Megascopically, the metabasic rocks are medium- to coarse-grained, showing massive or planar and linear arrangement of brownish green hornblende that imparts a gneissic fabric to the rocks. They show variable textures, *viz.* nematoblastic, occasionally granoblastic and micro-granular. Samples C1, B9, B15 and B20 are composed of variable proportions (vol.%) of green amphibole (17-42%), plagioclase (31-51%), clinopyroxene (11-19%), ortho-pyroxene (5-10%) and quartz (2 to 10%) and minor amounts of ilmenite. Apatite, Fe-sulphides and Cu-Fe sulphides are present as accessory minerals. Sample B9 also contains traces of tremolite and calcite. Tremolite often rims clinopyroxenes. In thin sections, green coloured amphiboles are usually euhedral or subhedral and more abundant than the yellowish brown secondary amphibole. The composition of plagioclase varies from An_{46} to An_{59} in the above mentioned samples. Subrounded grains of hypersthene show pleochroism from colourless to pale pink.

Sample B5 does not contain pyroxenes. Instead it is richer in hornblende (58%), poorer in plagioclase (20%) and contains abundant quartz (20%). Accessory minerals include apatite, ilmenite, Fe-sulphides, zircon and sphene. Alteration products in the form of chlorite, epidote, zoisite

Table 2. Modal proportion of minerals in the metamorphosed mafic-ultramafic rocks of the eastern sector of CMB (vol.%)

Sample	Hbl	Plg	Cpx	Opx	Qz	Ilm	Fs	Trace
B46	69.0	-	19.0	-	-	-	-	Apt, Zrc, Ilm, Fs
C1	33.5	36.0	12.0	8.4	9.4	0.8	-	Fs
B5	58.3	19.8	-	-	20.0	1.6	0.3	Apt, Zrc, Sph, Epd, Zoi, Trm
B9	23.8	41.9	18..0	7.6	6.9	1.5	0.3	Apt, Trm, Cc
B15	41.6	30.6	11.0	5.1	10.4	1.3	0.2	Apt, Mt, Cfs
B20	16.6	50.6	18.9	10.2	2.2	1.3	0.2	Apt
C14	55.8	28.6	-	-	4.4	2.1	-	Zrc, Aln, Fs, Trm, Cc

Note: B46 also contains 12.1% Scp; and C14 also contains 7.8% Bt and 1.3% Apt.

Abbreviations: Aln - allanite, Apt - apatite, Bt - biotite, Cc - calcite, Cfs - Cu-Fe-sulphides, Cpx - clinopyroxene, Epd - epidote, Fs - Fe-sulphides, Hbl - hornblende, Ilm - Ilmenite, Mt - magnetite, Opx - orthopyroxene, Plg - plagioclase, Qz - quartz, Scp - scapolite, Sph - sphene, Trm - tremolite, Zoi - zoisite

Table 3. Chemical composition (wt%) of minerals in metamorphosed mafic-ultramafic rocks of the eastern sector of CMB

	Hornblende							Tremolite			Biotite	Chlorite	Clinopyroxene					Orthopyroxene				Plagioclase						Scapolite	Epidote	Zoisite
Oxide	B46	C1	B5	B9	B15	B20	C14	B5	B9	C14	C14	B5	B46	C1	B9	B15	B20	C1	B9	B15	B20	C1	B5	B9	B15	B20	C14	B46	B5	B5
SiO_2	43.41	41.72	38.87	41.85	42.19	43.15	43.62	52.94	49.54	50.27	36.22	24.80	53.22	52.29	51.59	51.87	52.58	50.70	50.39	50.66	51.53	54.60	57.69	55.33	54.79	53.83	57.84	48.78	38.93	43.60
TiO_2	1.40	1.62	1.79	1.74	1.70	1.71	1.24	0.11	0.33	0.23	3.70	0.13	0.14	0.10	0.15	0.13	0.15	0.08	0.04	0.04	0.04	-	-	-	-	-	-	-	-	-
Al_2O_3	12.68	11.73	12.60	11.60	11.51	11.29	11.52	1.57	4.62	6.00	15.17	20.38	1.43	0.93	1.23	1.23	1.35	0.62	0.78	0.71	0.72	28.89	27.17	28.53	28.90	29.89	27.27	27.01	27.24	24.01
Cr_2O_3	0.20	0.04	0.15	0.05	0.06	0.15	0.07	0.00	0.02	0.01	0.04	-	0.05	0.02	0.02	0.01	0.02	0.00	0.01	0.01	0.01	-	-	-	-	-	-	-	-	-
FeO	15.25	19.52	20.44	19.50	19.69	17.67	17.33	19.50	15.54	14.32	19.65	31.38	8.63	11.94	12.99	12.49	10.96	32.59	33.03	33.10	30.78	0.06	0.09	0.08	0.10	0.03	0.15	0.06	7.97	0.20
MnO	0.24	0.19	0.31	0.15	0.20	0.133	0.26	0.15	0..14	0.17	0.08	0.26	0.30	0.35	0.29	0.35	0.29	0.99	0.79	0.99	0.71	-	-	-	-	-	-	-	-	-
MgO	10.31	8.27	7.19	8.45	8.31	9.66	10.02	11.28	12.87	14.00	11.36	6.82	12.73	11.85	11.37	11.44	12.32	14.82	14.87	14.78	16.57	0.00	0.00	0.00	0.00	0.00	0.00	0.01	0.05	0.00
CaO	11.98	11.47	11.26	11.39	11.30	11.36	11.44	12.46	12.79	11.74	00.02	0.10	23.85	22.48	22.04	22.07	22.46	0.49	0.58	0.55	0.49	10.92	8.71	10.45	10.77	11.88	8.54	15.27	23.45	26.35
Na_2O	1.98	1.55	1.63	1.59	1.75	1.70	1.41	0.08	0.32	0.57	0.11	0.10	0.37	0.32	0.28	0.27	0.31	0.00	0.00	0.00	0.01	5.36	6.56	5.74	5.49	4.83	6.77	4.99	0.00	0.07
K_2O	0.37	1.16	1.01	1.12	0.78	0.78	0.93	0.02	0.22	0.27	9.41	-	-	-	-	-	-	-	-	-	-	0.08	0.10	0.13	0.08	0.08	0.10	0.18	0.02	0.01
F	0.00	0.00	0.00	0.00	0.03	0.00	0.04	0.00	0.02	0.00	0.07	-	-	-	-	-	-	-	-	-	-	-	-	-	-	-	-	-	-	-
Cl	0.19	0.51	0.42	0.38	0.50	0.43	0.21	0.00	0.09	0..07	0.26	-	-	-	-	-	-	-	-	-	-	-	-	-	-	-	-	0.86	-	-
S	-	-	-	-	-	-	-	-	-	-	-	-	-	-	-	-	-	-	-	-	-	-	-	-	-	-	-	0.001	-	-
Total	98.02	97.80	95..68	97.83	98.04	98.04	98.09	98.100	96.49	97.62	96.07	83..97	100.73	100.27	99.95	99.86	100.42	100.30	100.51	100.83	100.87	99.92	100.31	100.26	100.13	100.53	100.67	97.17	97.65	94.21
Structural Formula																														
Si	6.420	6.334	6.069	6.334	6.370	6.437	6.457	7.811	7.356	7.221	5.505	5.661	1.976	1.977	1.965	1.972	1.973	1.984	1.972	1.977	1.982	2.464	2.575	2.487	2.467	2.420	2.574	2.421	1.973	2.207
Ti	0.156	0.185	0.210	0.198	0.193	0.192	0.138	0.012	0.037	0.024	0.423	0.022	0.004	0.003	0.004	0.004	0.004	0.002	0.001	0.001	0.001	-	-	-	-	-	-	-	-	-
Al	2.211	2.100	2.319	2.69	2.049	1.985	2.009	0.273	0.808	1.016	2.718	5.484	0.063	0.041	0.055	0.055	0.060	0.029	0.036	0.033	0.033	1.536	1.429	1.511	1.534	1.584	1.430	1.579	1.625	1.432
Cr	0.023	0.005	0.018	0.006	0.007	0.017	0.008	0.000	0.002	0.002	0.005	-	0.001	0.001	0.000	0.000	0.000	0.000	0.000	0.000	0.000	-	-	-	-	-	-	-	-	-
Fe	1.886	2.478	2.669	2.468	2.486	2.205	2.145	2.45	1.930	1.720	2.497	5.992	0.268	0.377	0.414	0.397	0.344	1.066	1.081	1.080	0.990	0.002	0.003	0.003	0.004	0.001	0.005	0.003	0.339	0.008
Mn	0.030	0.025	0.041	0.019	0.026	0.017	0.033	0.019	0.018	0.020	0.010	0.050	0.010	0.011	0.009	0.011	0.009	0.033	0.026	0.033	0.023	-	-	-	-	-	-	-	-	-
Mg	2.274	1.8733	1.674	1.906	1.871	2.147	2.210	2.480	2.849	2.997	2.573	2.320	0.705	0.668	0.646	0.648	0.689	0.864	0.868	0.859	0.950	0.000	0.000	0.000	0.000	0.000	0.000	0.001	0.004	0.000
Ca	1.898	1.865	1.883	1.846	1.828	1.816	1.815	1.969	2.035	1.806	0.003	0.024	0.949	0.910	0.899	0.899	0.903	0.021	0.024	0.023	0.020	0.528	0.416	0.503	0.519	0.572	0.407	0.812	1.273	1.427
Na	0.568	0.456	0.493	0.468	0.513	0.493	0.406	0.023	0.092	0.158	0.031	0.045	0..027	0.023	0.021	0.020	0.022	0.000	0.000	0.000	0.000	0.469	0.568	0.500	0.479	0.421	0.584	0.480	0.000	0.007
K	0.070	0.225	0.201	0.2166	0.151	0.149	0.175	0.004	0.041	0.049	1.825	-	-	-	-	-	-	-	-	-	-	0.005	0.006	0.007	0.004	0.004	0.005	0.011	0.001	0.001
F	0.000	0.002	0.000	0.000	0.015	0.000	0.017	0.000	0.009	0.000	0.034	-	-	-	-	-	-	-	-	-	-	-	-	-	-	-	-	-	-	-
Cl	0.047	0.131	0.112	0.099	0.128	0.110	0.053	0.000	0.023	0.016	0.066	-	-	-	-	-	-	-	-	-	-	-	-	-	-	-	-	0.072	-	-
S	-	-	-	-	-	-	-	-	-	-	-	-	-	-	-	-	-	-	-	-	-	-	-	-	-	-	-	0.000	-	-
Cation sum	-	-	-	-	-	-	-	-	-	-	-	-	4.002	4.011	4.013	4.007	4.004	4.000	4.009	4.006	4.000	5.004	4.997	5.012	5.008	5.001	5.006		5.216	5.081
Mg(Mg+Fe)	0.55	0..43	0.39	0.44	0.43	0.49	0.51	0.51	0.60	0.64	0.51	0.28	0.72	0.64	0.61	0.62	0.67	0.45	0.45	0.44	0.49	-	-	-	-	-	-	-	-	-
En	-	-	-	-	-	-	-	-	-	-	-	-	0.37	0.34	0.33	0.33	0.36	0.44	0.44	0.44	0.49	-	-	-	-	-	-	-	-	-
Wo	-	-	-	-	-	-	-	-	-	-	-	-	0.49	0.47	0.46	0.46	0.47	0.01	0.01	0.01	0.01	-	-	-	-	-	-	-	-	-
Fs	-	-	-	-	-	-	-	-	-	-	-	-	0.14	0.19	0.21	0.20	0.18	0.55	0.55	0.55	0.50	-	-	-	-	-	-	-	-	-
An-content	-	-	-	-	-	-	-	-	-	-	-	-	-	-	-	-	-	-	-	-	-	0.53	0.42	0.50	0.52	0.57	0.41	-	-	-

Note: All hornblende, biotite, pyroxenes, plagioclase and scapolite compositions are averages of 5 analyses each; tremolite, chlorite and epidote compositions are averages of 2 analyses each; zoisite composition is a single analysis.

Structural formula for hornblendes and tremolites are calculated on the basis of 13 tetra- and octahedrally coordinated cations (exluding Ca, Na and K). Biotite structural formula is calculated on the basis of 22O-(Cl+F), and chlorite structural formula is on the basis of 28O. Structural formula for pyroxenes are calculated on the basis of 6 oxygens and plagioclase, epidote and zoisite are calculated on the basis of 8 oxygens. Scapolite structural formula is calculated on the basis of 4(Si, Al) cations.

and tremolite are also present. Both twinned and untwinned plagioclases are present, the former showing lamellar twinning. Plagioclases are present both as inclusions within amphibole and as discrete grains. The inclusions are untwinned and sericitised. Plagioclase composition ranges between An_{40} and An_{44}. Quartz and some feldspar show effects of crushing and granulation. Rarely extension (pull apart) cracks have developed which have been later filled by crystallisation of amphibole. The rock is also pervasively affected by brittle fractures, which are developed parallel to the preferred orientation of other mafic minerals. These features probably suggest that the country rock was subjected to extension first under a ductile and later under a brittle regime.

The sheared metabasic rock is fine- to medium-grained, thinly foliated, and shows development of mortar texture and micro-shear planes filled with alteration products. Green hornblende (56%), plagioclase (29%), brown biotite (8%) and quartz (4.4%) are the major mineral components, whereas, ilmenite and apatite are present in minor amounts. Plagioclase and quartz occur around large intergrowths of hornblende and biotite. Weakly zoned plagioclase also occurs as inclusions within amphibole. Plagioclase composition ranges between An_{40} and An_{43}. Other accessory minerals include zircon, allanite and Fe-sulphides. Tremolite associated with quartz and hornblende or biotite is present in traces, and traces of calcite inclusions are present in some biotites. The preferred orientation of brown biotite imparts micro-lineation/planar fabric to the rock. In thin section, alteration of hornblende to green biotite along grain boundary shows release of iron along the cleavage traces. Small granular plagioclases are mostly untwinned, but a few show lamellar or, rarely, pericline twinning. Ilmenite occurs as primary skeletal grains, and granular magnetite occurs as a secondary product of late alteration of mafic minerals.

Mineralogical study shows that the primary amphibole compositions of the mafic-ultramafic suite range from hornblende to pargasitic hornblende. There is a positive correlation between the edenitic content (represented by [Na+K]) and the tschermakitic content (represented by $0.5[Al_T-\{Na+K\}]$, Al_T being Al in the tetrahedral site) (Figs. 2A,B). Ti is also positively correlated with each of these components (Figs.2C,D). The hornblendes from the anorthosites (Sen and Bhattacharya, 1985) and from the sheared metabasic are the most and the least pargasitic, respectively. The secondary amphiboles are tremolitic with low edenite and tschermakite contents (Figs. 2A,B).

Although there are some intra-sample variations, the Mg# (atomic Mg/[Mg+Fe]) of clinopyroxenes show a positive correlation with the Mg#'s of hornblendes and orthopyroxenes (Figs.3A,B) indicating that the Fe-Mg exchange K_D is constant between coexisting ferromagnesian minerals. Except the sheared metabasic sample C14, Mg# of hornblendes of other samples are also positively correlated with the An-content of plagioclase of the corresponding samples (Fig.3C). The Mg#'s of the pyroxenes and hornblendes, and the An-content of plagioclase of sample B20 are distinctly higher than those of the other metabasic samples. The ultramafic sample B46 shows the highest Mg#'s of hornblendes and clinopyroxenes (Fig. 3A). In general, the positive correlations of the coexisting phases (Fig.3) indicate that the rocks experienced similar conditions of metamorphism approaching equilibrium.

The scapolites of the ultramafic sample B46 are similar in composition to the scapolites in anorthosites and granulites (Sen and Bhattacharya, 1985), but contain less Ca than the scapolites in calc-gneisses (Sen and Bhattacharya, 1993). The ilmenites of the metabasics show a uniform composition, but the ilmenites of the sheared metabasic sample C14 contain higher Mn than those of the other metabasics.

GEOCHEMISTRY

Seven representative samples of the metamorphosed mafic-ultramafic rocks were chemically analysed both for major and trace elements by XRF on pressed powder pellets at the University of Leicester, U.K. Powdering of the samples was carried out by passing through a tungsten-carbide crusher and subsequent grinding in an agate mortar. Several natural standards viz. MRLG-1, JP-1, W-1 and BOB–1 were also analysed simultaneously to check the precision and accuracy of analytical data. The chemical and normative compositions of the metamorphosed mafic-ultramafic rocks are given in Table 4 and the trace elements in Table 5.

Chemically, the metabasic rocks are essentially tholeiitic in composition varying from quartz normative to olivine normative tholeiites (Table 4). On the basis of abundance of TiO_2 and incompatible elements, these rocks have been classified into two distinct groups - viz. (i) Low-Ti (TiO_2 < 2 wt%) metabasics, moderately-rich in incompatible elements, and (ii) High-Ti (TiO_2 > 2 wt%) metabasics, enriched in incompatible elements; the latter being rich in K_2O and P_2O_5 as well. A strong negative correlation between MgO and total iron (Fig. 4) and V (Fig. 5B), and a positive correlation of Ni (Fig.5A) of the metabasic rocks, demonstrate fractional crystallisation with separation of olivine, high-Ca clinpyroxene and plagioclase from the

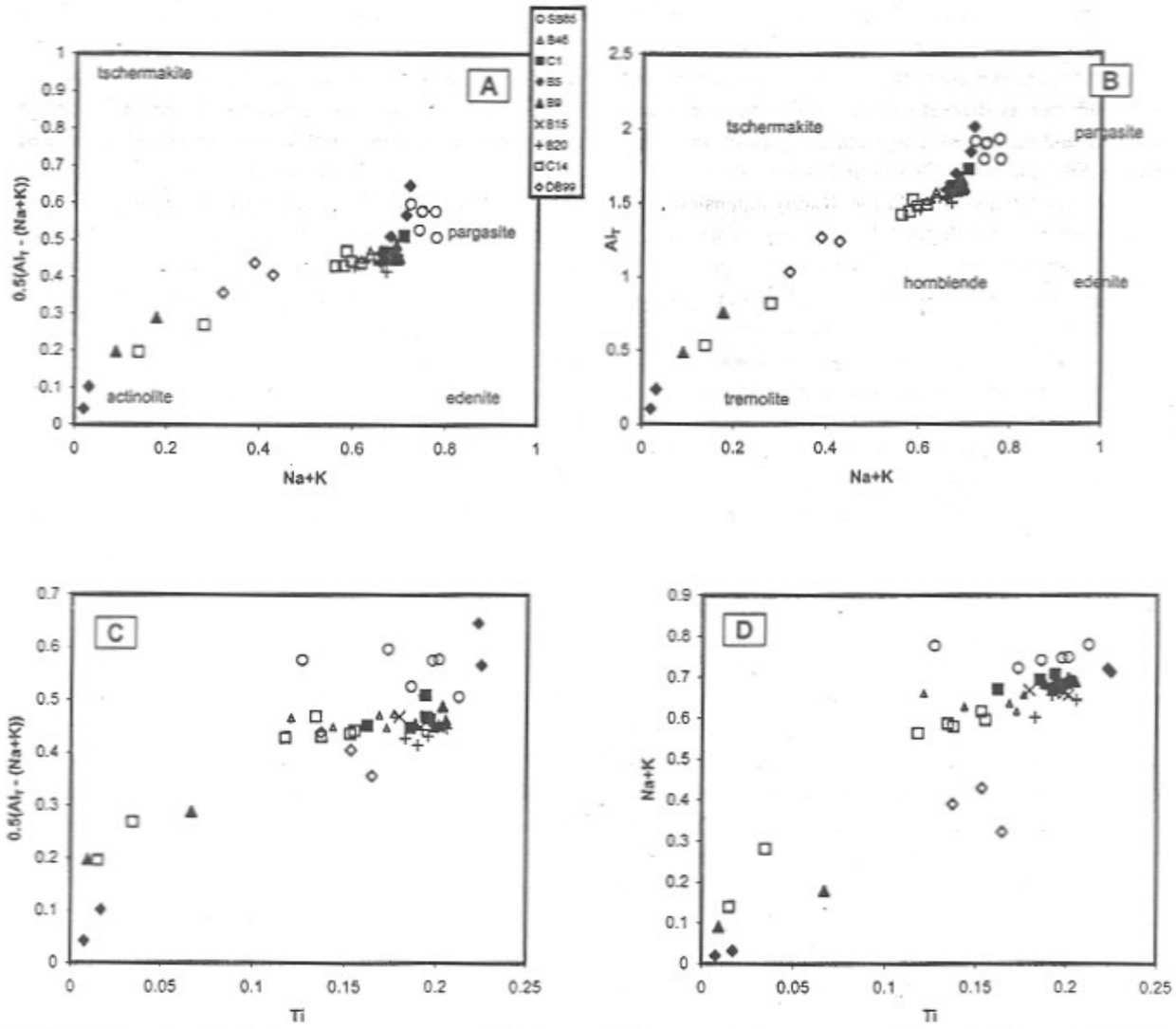

Fig.2. Variation of Na+K (edenite component) with (**A**) 0.5[Al_T-{Na+K}] (tschermakite component), and (**B**) Al_T (Al in tetrahedral site); and variation of Ti with (**C**) 0.5[Al_T-{Na+K}], and (**D**) Na+K in the amphiboles of the ultramafic and metabasic rocks in and around the Bengal anorthosite massif. All values are in atomic formula units. Symbols used for each rock from which amphiboles were analysed are shown. Composition of amphiboles from the massif anorthosite (SB85) near Saltora (Sen and Bhattacharya, 1985), and those from the amphibolite country rock (DB99) near Tulin-Jhalida area, southwest of the present study area (Das and Bhattacharyya, 1999) are also presented for comparison.

parent magma. Similarly, a progressive increase in Rb with K_2O (Fig. 5C), Rb and Y with Zr (Figs. 6A,B), Nb and La with TiO_2 (Fig. 6C,D), and a wide range in $(La/Nd)_N$ ratios of the metabasics (1.08 and 2.08) also support this conclusion. The AFM plot of the metabasics shows a typical tholeiitic trend with progressive enrichment of iron (Fig. 7). Enrichment of incompatible elements in the high-Ti metabasic sample C14 by a magnitude of 3 to 5 times greater than the low-Ti type (Table 5), favour chemical affinity with the oceanic island basalt (OIB) both in terms of abundance (Table 5) and trend (cf. Sun and McDonough, 1989). Variation of incompatible elements in the high-Ti metabasic shows strong positive anomalies of Ba, K, P and Ti, and negative anomalies of Th, Sr and Zr in the high-Ti metabasic rock (Fig. 8). Negative anomalies of lithophile elements, viz. Th and Zr, in particular, suggest a source other than crustal contamination. In contrast, the low-Ti metabasics are characterised by relatively flat incompatible element patterns except for a negative Sr-anomaly (Fig. 8), suggestive of plagioclase controlled-fractional crystallisation. Lower

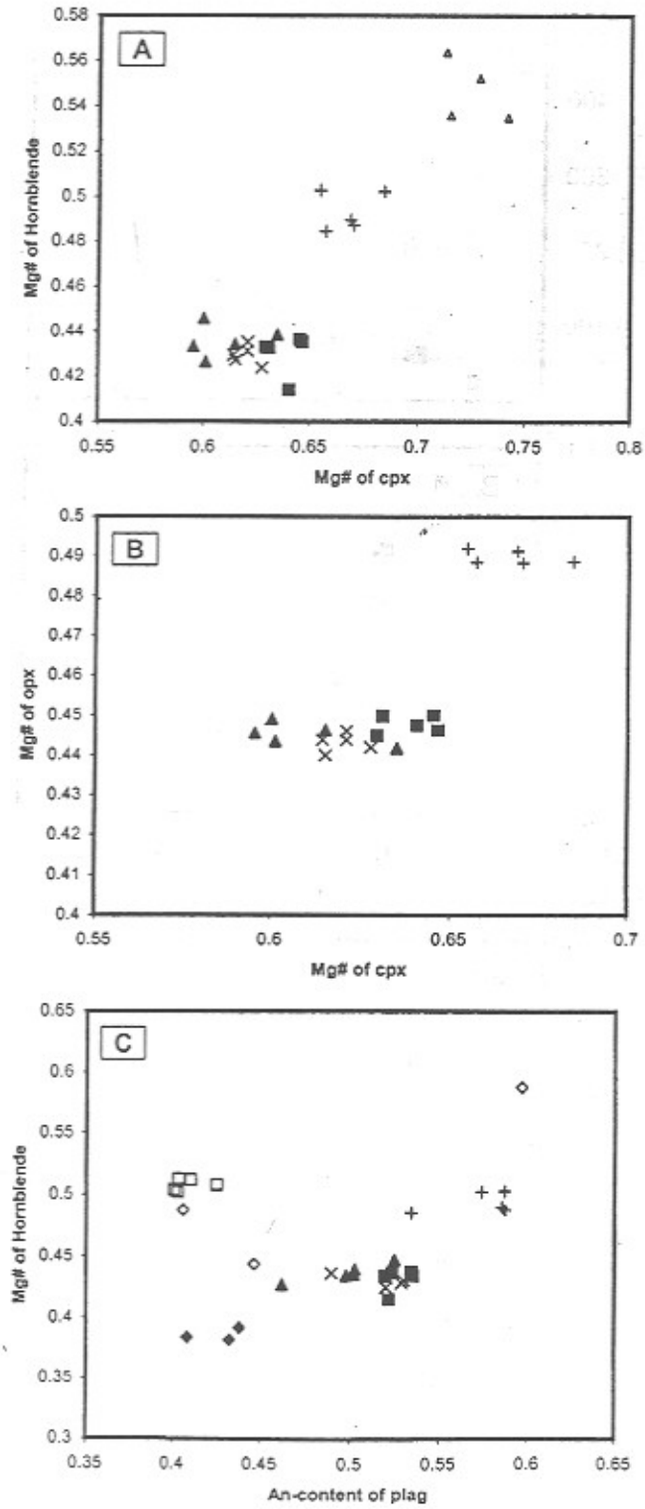

Fig.3. Variation of Mg# (atomic Mg/[Mg+Fe]) of clinopyroxenes with (A) Mg# of hornblendes and (B) Mg# of orthopyroxenes; and (C) variation of An-content of plagioclases with the Mg# of hornblendes of the metabasic rocks in and around the Bengal anorthosite massif. Symbols are as in Fig. 2.

Table 4. Major oxide composition (wt%) of metamorphosed mafic-ultramafic rocks in the eastern sector of CMB

Oxide	Ultra-mafic (meta)	Low-Ti metabasic					High-Ti meta-basic
	B46	C1	B5	B9	B15	B20	C14
SiO_2	43.95	48.37	47.31	46.76	47.50	46.46	45.30
TiO_2	1.09	1.45	1.84	1.62	1.59	1.24	2.99
Al_2O_3	11..09	11.64	11.23	12.90	12.45	13.75	11.54
Fe_2O_3	3.06	3.29	3.91	2.25	3.44	1.38	3.25
FeO	8.99	11.14	11.60	11.43	10.65	10.57	11.75
MnO	0.20	0.20	0.22	0.21	0.21	0.20	0.18
MgO	10.10	5.67	4.93	5.78	5.68	6.91	7.79
CaO	14.86	10.01	9.16	10.80	10.32	11.78	7.89
Na_2O	1.85	1.81	2.02	2.24	2.08	2.07	1.52
K_2O	0.28	0.53	0.70	0.34	0.35	0.21	2.34
P_2O_5	0.10	0.21	0.24	0.24	0.22	0.19	0.77
Total	95.57	94.32	93.16	94.57	94.49	94.76	95.32
FeOt*	11.74	14.10	15.12	13.45	13.75	11.81	14.67
Mg'**	60.52	41.75	36.76	43.37	42.42	51.05	48.62
CaO/Al_2O_3	1.34	0.86	0.82	0.84	0.83	0.86	0.68
K_2O/Na_2O	0.15	0.29	0.35	0.15	0.16	0.10	1.54
CIPW Normative composition							
qz	0	5.46	4.81	0	3.15	0	0
or	1.66	3.13	4.14	2..1	2.07	1.24	13.83
ab	6.39	15.31	17...09	18.95	17.60	17.51	12.86
an	21.14	22.07	19.51	24.14	23.60	27.61	17.76
ne	5.02	0	0	0	0	0	0
di	42.12	20..03	20.32	23.18	21.66	24.45	13.39
hy	0	19.88	17.57	18.52	17.89	12.01	19.76
ol	12.52	0	0	0.87	0	7.13	5.75
mt	4.44	4.77	5.67	3.26	4.99	2	4.71
ch	0.25	00	0	0	0	0	0
ilm	2.07	2.75	3.49	3.08	3.02	2.35	5.68
apt	0.24	1.26	0.57	0.57	0.52	0.45	1.82

Analyst: N.G. Marsh, Leicester.
*Total Fe calculated as FeO; **Mg' = 100 x Mg/(Mg+total Fe)
Abbreviations: qz - quartz, or - orthoclase, ab - albite, an - anorthite, ne - nepheline, di - diopside, hy - hypersthene, ol - olivine, mt - magnetite, ch - chromite, ilm - ilmenite, apt - apatite

Ce/Nb and Zr/Nb, and higher Zr/Y, Ba/Sr, Nb/Y and Ti/Y ratios of the high-Ti metabasic compared to the low-Ti metabasic distinguish the two groups of metabasics (Table 5), and relate them to have been generated possibly from different source regions.

The ultramafic rock (B46) is characterised by high MgO, Ni and Cr, and low SiO_2, TiO_2, P_2O_5, K_2O and incompatible elements, viz., Rb, Ba, Zr, Nb and LREE, when compared with the metabasic rocks. Absence of normative hypersthene and presence of normative diopside and olivine as well as low silica content suggests this to be possibly wherlitic in

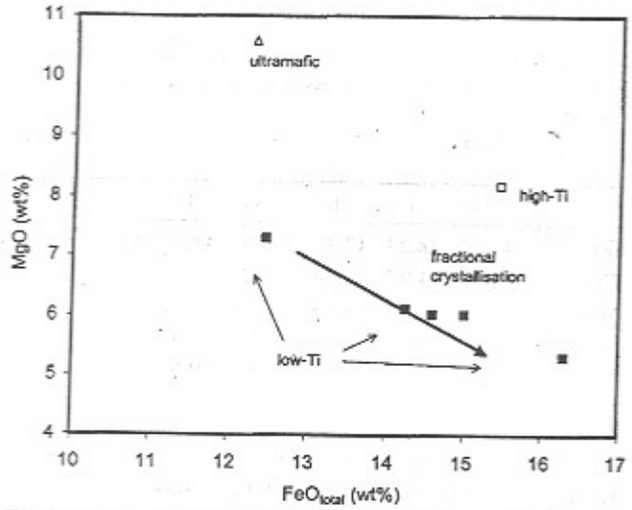

Fig.4. Variation of total FeO with MgO in the metabasics and ultramafic rocks of the eastern sector of the Chotanagpur mobile belt (CMB). Solid square: low-Ti metabasic, open square: high-Ti metabasic, and triangle: ultramafic rock.

composition. It is a nepheline normative rock and appears to have been derived from a depleted mantle source. The variation of incompatible elements of ultramafic rock is noted with positive anomalies of Th, Sr and Ti, and negative anomalies of Nb and Nd (Fig. 8), indicating minor contamination by the gneissic basement. The K/Rb ratio (365) of the ultramafic rock is comparable to the metabasics. However, Ti/Y, Zr/Nb and Ce/Nb ratios of the ultramafic rock are greater than the metabasics (Table 5).

The discriminant diagram of Cr versus Y supports that the metabasics are formed in a 'within plate' (WPB) environment, and show a strong progressive enrichment of Cr with the decrease of Y (Fig. 9). The Zr/Nb and Nb/La ratios of the metabasics are also similar to the ratios for continental tholeiites of Condie (1989) (Table 5). The ultramafic rock plots within the field of island arc basalt (IAB) (Fig. 9) and its Zr/Nb and Nb/La ratios are similar to continental rift alkali basalts (Table 5). The variations in immobile elements like Ti-Zr-Y of the low-Ti metabasics (Fig. 10) show affinity with the ocean floor basalt (OFB), but plot within the field of continental flood basalts demarcated for Deccan basalts. In contrast, the high-Ti metabasic plots within the field of oceanic island basalt and continental basalt (OIB and CB). Similarly, the FeO_t-MgO-Al_2O_3 discriminant diagram indicates that the high-Ti metabasic and ultramafic rock plot within the field of basalts formed in oceanic island, whereas the low-Ti metabasics are transitional between the oceanic island and continental basalts (Fig.11).

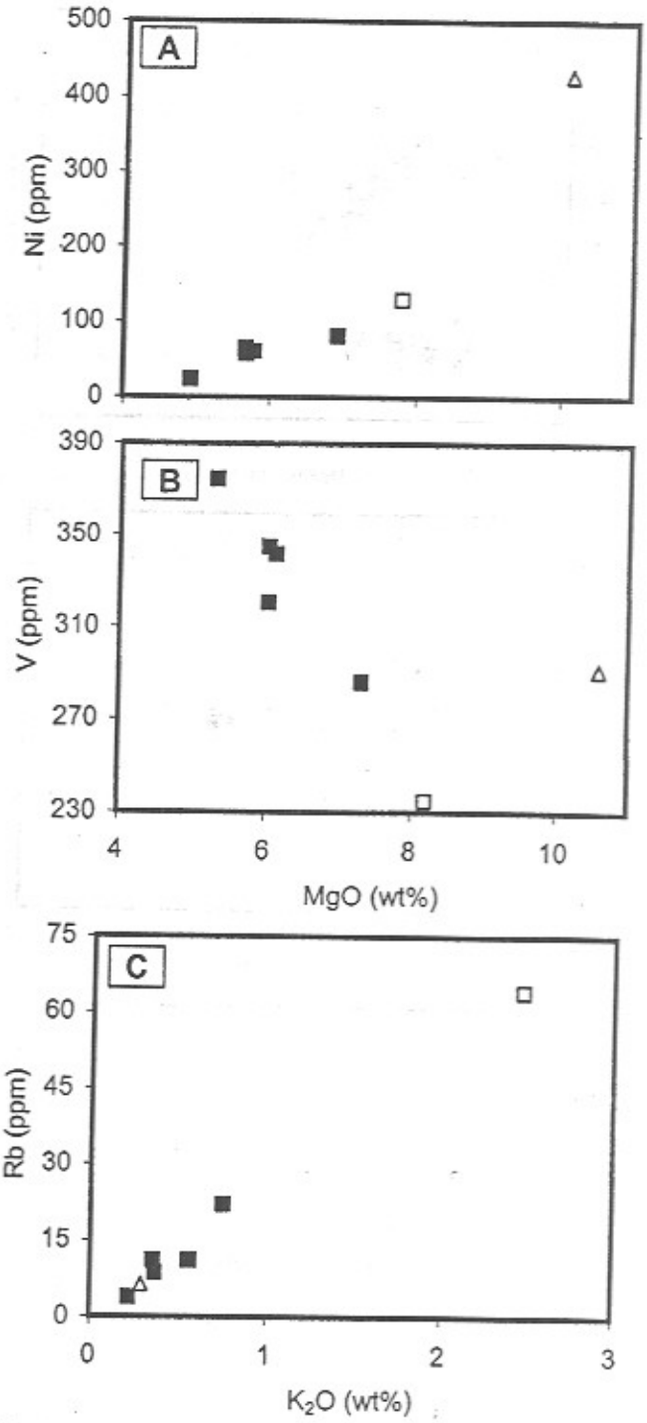

Fig.5. MgO *vs* V(**B**) and Ni (**A**); and K_2O *vs* Rb (**C**) of metabasic and ultramafic rocks of CMB. Key as in Fig.4.

DISCUSSION

The chemical data of the low-Ti metabasics demonstrate that the parent magma from which these were derived underwent fractionation with separation of olivine, high-Ca clinopyroxene and plagioclase, as indicated by a progressive

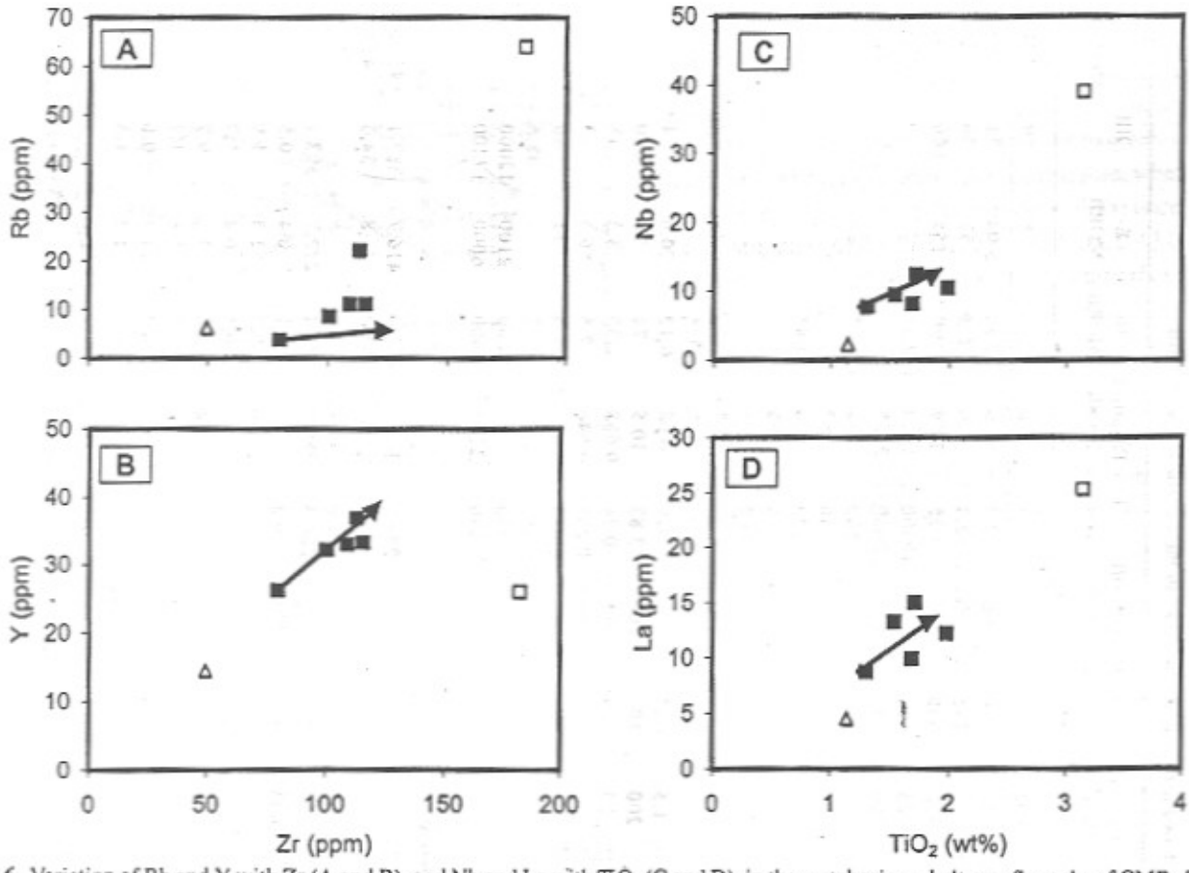

Fig.6. Variation of Rb and Y with Zr (A and B), and Nb and La with TiO_2 (C and D), in the metabasic and ultramafic rocks of CMB. The fractional crystallisation paths (lines with arrows) starting from B20 have been calculated using trace element K_D's from Green (1994) and the Rayleigh fractionation equation. Key as in Fig. 4.

enrichment of Fe and V, and a reciprocal decrease of Mg and Ni. The fractional crystallisation relation among the low-Ti metabasics can be modelled (Fig. 4) by considering the highest-Mg sample (B20) as the parent and fractionating olivine, high-Ca clinopyroxene and plagioclase in a 7:19:24 proportion at 1 bar and 2% increments, while keeping the major element crystal-melt distribution coefficients (K_D) in agreement with experimental values (cf. Roeder and Emslie, 1970; Grove et al. 1992). Using a bulk crystal-melt K_D for trace elements, calculated from the above-mentioned proportion of crystallising phases, it could be shown that the other low-Ti rocks may be derived by fractional crystallization of B20. The agreement between the measured and calculated concentrations of high field-strength (HFS) elements Zr, Y, Ti, Nb and La (Figs. 6B,C, D), and large-ion lithophile (LIL) elements K and Ba are excellent, whereas Rb (Fig. 6A) and Th are within permissible range. It is interesting to note that the trends for the LIL elements have been preserved despite obvious metamorphism in these rocks.

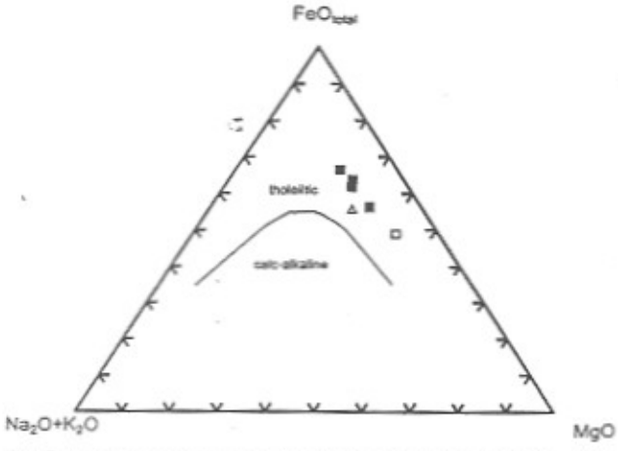

Fig.7. AFM diagram of the mafic-ultramafic rocks of CMB. Key as in Fig. 4. The boundary between tholeiitic and calc-alkaline rocks is from Irvine and Baragar (1971).

Two geothermometers based on mineral chemistry can be applied to these rocks to estimate the temperature of metamorphism: the two-pyroxene thermometer of Lindsley

Table 5. Trace element concentration (ppm) of metamorphosed mafic-ultramafic rocks in the easter

Trace Elements	Ultra-mafic (meta)	Low-Ti metabasics					High-Ti meta-basic	Island Arc basalt	Cont. rift tholeiite	High-Al tholeiite	Cont. rift alkali basalt	Cl chondri	OIB	T-MORB
	B46	C1	B5	B9+	B15	B20	C14	1	2	3	4	5	9	10
Rb	6.3	11.1	22.1	11.1	8.6	3.8	64.1	5	31	10	200	2.3	31	3.1
Ba	71.6	147.5	154.6	131.5	113.6	94.7	1014.7	50	17	115	700	2.4	350	31
Sr	172	133.2	167.7	146.7	131.3	152.1	481.2	225	350	330	1500	7.25	660	101
Ni	428.3	64.7	24.2	61	57.6	81.6	129.2	25	85	25	100	10500		106.4
Cr	1139.9	93.3	19.3	135.4	116.5	251.6	284.8	50	160	40	400	2650		311
Co	63.4	58.5	55.2	56.3	63.9	57.6	59.1					500		48.9
V	291.5	320.6	374.8	342	3345	286	235					56		328
Cu	66.6	70.9	49.6	86.4	90.7	104.7	42.7					120		
Zn	90.5	117.2	83.9	109.4	114.3	82.8	152.9					310		
Ga	16.6	17.3	19.6	19.3	19.8	17.3	22					9.2		
Y	14.5	33	36.9	33.3	32.2	26.2	26					1.57	29	
Sc	40.8	42.8	43.8	53	52	48	24.3					5.92		42.5
Th	1.2			3.8	1.1	1	2.8	0.5	1.5	1.11	4	0.029	4	
Zr	49.8	109.2	113.1	115.7	100.5	80.1	182.6	60	200	100	800	3.82	280	
Nb	2.3	9.4	10.5	12.4	8.2	7.7	39.1	1	25	5	35	0.24	48	
La	4.5	13.2	12.2	15	9.9	8.7	25.3	3.3	33	10	54	0.237	37	4.96
Ce	15	24.1	29.9	25.8	15.7	24.5	60.3					0.613	80	
Nd	6	12.5	19	17.7	10.6	15.9	30.3					0.457	38.5	
K	2300	4400	5800	2800	2900	1700	19400					550	12000	1289
Ti	6535	8693	11031	9712	9532	7434	17925					440	17200	
								Ratios						
K/Rb	365.1	396.4	262.4	252.3	337.2	447.4	302.7					239.1	387.1	415.8
K/Ba	32.1	29.8	37.5	21.3	25.5	18.0	19.1					229.2	34.3	41.6
Ni/Co	6.8	1.1	0.4	1.1	0.9	1.4	2.2					21.0		2.2
Ti/Y	450.7	263.4	298.9	291.7	296.0	283.7	689.4					280.3	593.1	
Ba/Sr	0.4	1.1	0.9	0.9	0.9	0.6	2.1	0.2	0.05	0.3	0.5	0.3	0.5	0.3
$(La/Nd)_N$	1.4	2.0	1.2	1.6	1.8	1.1	1.6					1	1.9	
Nb/Y	0.2	0.3	0.3	0.4	0.3	0.3	1.5					0.2	1.7	
Zr/Y	3.4	3.3	3.1	3.5	3.1	3.1	7.0					2.4	9.7	
Ce/Nb	6.5	2.6	2.8	2.1	1.9	3.2	1.5					2.6	1.7	
Zr/Th	41.5			30.4	91.4	80.1	65.2	120.0	133.3	90.1	200.0	131.7	70.0	
Nb/La	0.5	0.7	0.9	0.8	0.8	0.9	1.5	0.3	0.8	0.5	0.6	1.0	1.3	
Zr/Nb	21.7	11.6	10.8	9.3	12.3	10.4	4.7	60.00	8.0	20.0	22.9	15.9	5.8	

1 to 4 - after Condie, 1989 (p.210); 5,6 - after McDonough and Sun, 1995; 7 to 9 - after Sun and McDohough, 1989; *after Hofmann(average of means in Table 3).

CMB samples were analysed by N.G. Marsh, Leicester.

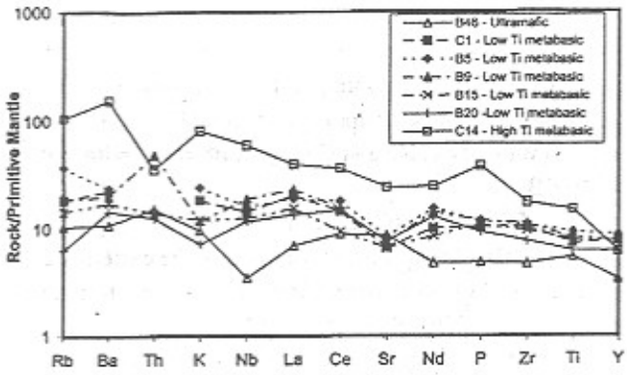

Fig.8. Primitive mantle-normalised (McDonough and Sun, 1995) incompatible element variation of the metabasic and ultramafic rocks from the eastern sector of CMB.

(1983), and the hornblende-plagioclase equilibrium thermometer of Holland and Blundy (1994). At a pressure of 5 kb, the two-pyroxene thermometer yields a temperature of 643 ±15°C, whereas, the hornblende-plagioclase thermometer (edenite-tremolite formulation in the presence of quartz) yields a higher temperature of 781± 22°C. Increases in Ti and octahedral Al in hornblende usually correspond to an increase in pressure. In the absence of garnet in these rocks, the Al content of hornblende is one of the very few pressure sensors in these rocks. Using the barometric formulation of Anderson and Smith (1995), the hornblende composition of these rocks yield pressures between 3.8 and 5.4 kb with an average of 4.7 kb at temperatures calculated with the hornblende-plagioclase thermometer. These pressures and temperatures possibly represent the post-peak metamorphic equilibrium conditions and correspond to high-grade amphibolite to granulite facies conditions. The temperatures are comparable, whereas, the pressures are slightly lower but overlap with the uncertainties of the estimates (680 ± 20° C, 6 ± 1 to 6.8 ± 0.4 kb) of Sen and Bhattacharya (1985, 1993) for the country rocks around Saltora.

The low-Ti metabasics show chemical affinity transitional between the ocean floor basalts (OFB) and analogues of continental flood basalts (CFB) viz. Deccan basalts (Fig. 10). These metabasics show a close chemical similarity with transitional basalts derived from T-MORB (cf. Schilling et al. 1983; and Table 5).

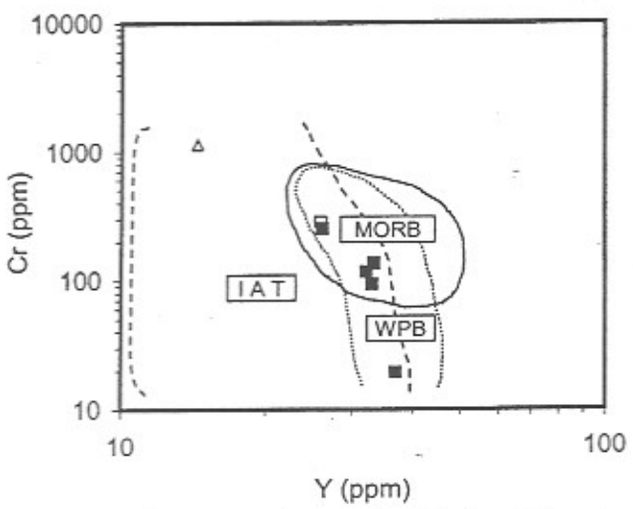

Fig.9. Cr *vs* Y discriminant diagram of metabasic and ultramafic rocks of CMB. The fields of basaltic rocks are after Pearce (1980). MORB - Mid-oceanic ridge basalt (field marked by solid line), IAT- Island arc tholeiite (field marked by dashed line), and WPB - within plate basalt (field marked by dotted line). Key as in Fig. 4.

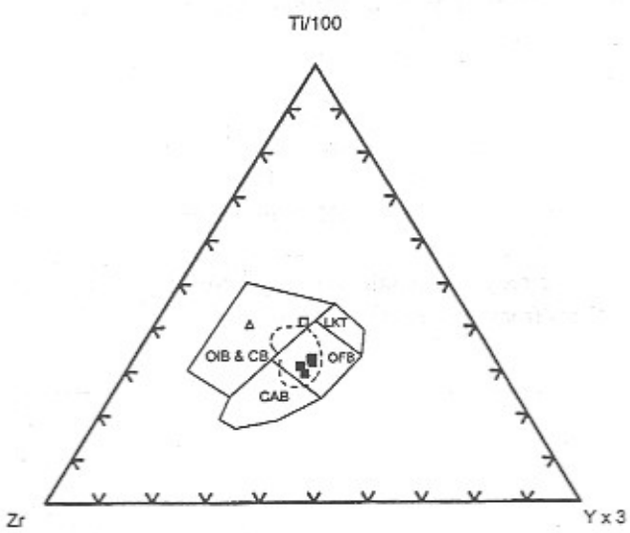

Fig.10. Ti-Zr-Y discriminant diagram of metabasic and ultramafic rocks of CMB. The fields of basaltic rocks are after Pearce and Cann (1973). OIB - oceanic island basalt, CB - continental basalt, LKT - low K-tholeiite, OFB - ocean floor basalt, and CAB - calc-alkaline basalt. The field shown by dashed line indicates composition of Deccan basalts from Mahableshwar (Najafi et al. 1981). Key as in Fig. 4.

The high-Ti metabasic rock is enriched in incompatible elements and shows an affinity with OIB. It may have been derived from E-MORB or a recycled mantle source fed by subducted oceanic crust. Thus the relative distribution of incompatible elements in the metabasic rocks reflects a difference in the source of magma generation in the mantle. The low-Ti metabasics were possibly derived as a result of high degree of partial melting (decompression melting) of a

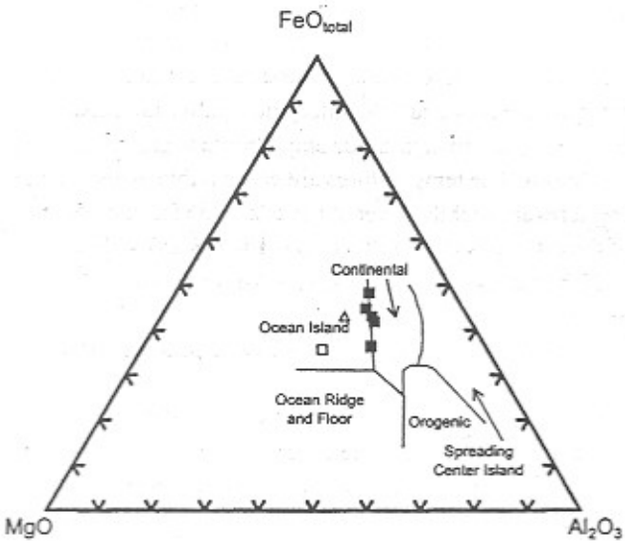

Fig.11. FeO_t-MgO-Al_2O_3 discriminant diagram of metabasic and ultramafic rocks of CMB. The fields of basaltic rocks are after Pearce and Cann (1973). Key as in Fig.4.

T-MORB-type mantle source, noted by their extensive occurrence throughout the CMB, whereas, the high-Ti metabasic rock having limited occurrence and reported first time, was generated by low degree of partial melting of enriched recycled mantle with high Nb concentration or perhaps from a plume derived source.

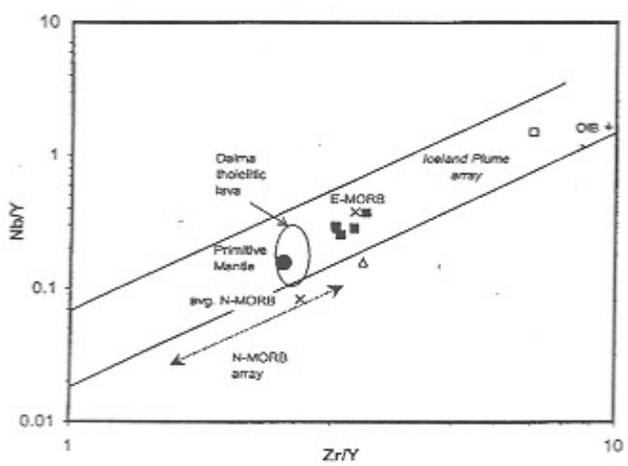

Fig.12. Nb/Y – Zr/Y discriminant plot for mafic and ultramafic rocks from the Chotanagpur mobile belt (this study) and Dalma volcanics (cf. Roy et al. 2002). Key as in Fig. 4. Note that all mafic rocks of CMB fall within the plume array of basalts from Iceland (cf. Fitton et al. 1997). Data for primitive mantle (solid circle) is from McDonough and Sun (1995), and data for OIB (plus) and E- and N-type MORB (crosses) are from Sun and McDonough (1989).

The depleted nature of the ultramafic rock with comparable trace element contents of Rb, Ba, Sr, Y, Th and Ce to the low-Ti metabasics points it to a mantle source of E-MORB composition (Table 5). However, low concentration of Sc, Nb and Ce is in conformity with that of N-MORB.

Bimodal, within-plate mafic-ultramafic magmatism (tholeiitic and alkaline ultramafic type) at the eastern sector of CMB in Mesoproterozoic time is analogous to plume-generated (viz. Kerguelen hot spot) Phanerozoic magmatism that generated the Rajmahal tholeiites and the ultrapotassic mafic-ultramafic intrusives of Damodar valley coal fields (Kent et al. 1997) in an extensional tectonic regime accompanied with crustal thinning. It is suggested that a similar tectonic environment may have existed during Mesoproterozoic time in an intra-cratonic rift setting that induced melting of the lithosphere by heat from a hot spot close to the eastern Indian craton. Evidently, in a Nb/Y-Zr/Y discriminant plot (Fig. 12), the mafic rocks of CMB fall within the field of the plume array (Iceland) along with the adjoining mafic-ultramafic suite of Dalma volcanics of Singhbhum Proterozoic province (Roy et al. 2002) that developed in an extensional tectonic regime (Bose, 2000).

The Mesoproterozoic plume was possibly responsible for rifting and a global thermal event (1.7-1.6 Ga, Peucat et al. 1997; Oliver and Fanning, 1997) that affected a huge landmass comprising Antarctica, Southwest Australia and Eastern India — joined together prior to the breakup of Gondwanaland. This thermal event has left behind a wide magmatic impression in the eastern Indian shield margin, e.g. Eastern Ghats Mobile Belt (1.6 Ga, Mezger and Cosca, 1999), Singhbhum Crustal Province (1.68-1.6 Ga, Sarkar et al. 1989; Sengupta et al.1994; Roy et al. 2002), and Chotanagpur Mobile Belt as evidenced by charnockitisation, migmatisation and granitic activity (1.74-1.6 Ga, Pandey et al. 1986; Ray Barman et al. 1990; Ray Barman and Bishui, 1994). The event is synchronous with the mantle isochrons (Brooks et al. 1976; Brooks and Hart, 1978) at which major mantle fractionation event occurred causing heterogeneities with respect to its Pb and Sr isotopes in the southern hemisphere (viz. Dupal anomaly). Thus the plume-related mafic-ultramafic intrusives both in the Dalma and the CMB in the eastern continental margin of India manifest as a part of the global thermal event involving lithospheric thinning, rifting, sedimentation, large scale mantle derived magmatism of mafic-ultramafic-anorthosite, granulite facies metamorphism, migmatisation accompanied with crustal anatexis, and emplacement of peraluminous granites. Magmatism in the CMB, however, continued for a protracted

period until Early Tertiary (Ghose and Mukherjee, 2000), giving evidence of reactivation of the Central Indian Son-Narmada geosuture linking with the Damodar valley since late Palaeoproterozoic time.

Acknowledgments: We are highly thankful to Prof. A.D. Saunders for XRF analyses of the samples at the Leicester, U.K. The award of Emeritus Fellowship to one of the authors (NCG) by the U.G.C., New Delhi, is gratefully acknowledged.

References

Anderson, J.L. and Smith, D.R. (1995) The effects of temperature and f_{O_2} on the Al-in-hornblende barometer. Am. Min., v.80, pp.549-559.

Armstrong, J.T. (1995) CITZAF - A package for correction programs for the quantitative electron microbeam x-ray analysis of thick polished materials, thin-films and particles. Microbeam Analysis, v.4, pp.177-200.

Bhattacharyya, P.K. and Mukherjee, S. (1987) Granulites in and around the Bengal anorthosite, eastern India: genesis of coronal garnet and evolution of the granulite-anorthosite complex. Geol. Mag., v.124, pp.21-32.

Bose, M.K. (2000) Mafic-ultramafic magmatism in the eastern Indian craton – A review. Geol. Surv. India Spec. Publ., no.55, pp.227-258.

Bose, M.K. and Roy, A.K. (1966) Co-existing iron titanium oxide minerals in norites associated with anorthosites of Bengal, India. Econ. Geol., v.61, pp.555-562.

Brooks, C. and Hart, S.R. (1978) Rb-Sr mantle isochrons and variations in the chemistry of Gondwanaland's lithosphere. Nature, v.271, pp.220-223.

Brooks, C., Hart, S.R., Hofmann, A. and James, D.E. (1976) Rb-Sr mantle isochrons from oceanic regions. Earth Planet. Sci. Lett., v.32, pp.51-61.

Condie, K.C. (1989) Plate Tectonics and Crustal Evolution. Pergamon Press, Oxford, 475p.

Das, A. and Bhattacharyya, C. (1999) Amphibolites from Tulin-Jhalida area, Puruliya District, West Bengal. Indian Jour. Geol., v.71, nos.1 and 2, pp.143-161.

Fitton, J.G., Saunders, A.D., Norrey, M.J. and Hendarson, B.S. (1997). Thermal and chemical structure of the Iceland plume. Earth Planet. Sci. Lett., v.153, pp.197-208.

Ghose, N.C. (1983) Geology, tectonics and the evolution of the Chhotanagpur granite gneiss complex, Eastern India. *In*: S. Sinha-Roy (Ed.), Structure and Tectonics of Precambrian Rocks of India, Recent Researches Geol., v.10, pp.211-247, Hindustan Publ. Co., Delhi.

Ghose, N. C. (1992) Chhotanagpur gneiss-granulite complex, Eastern India: Present status and future prospects. Indian Jour. Geol., v.64, pp.100-121.

Ghose, N.C. and Mukherjee, D. (2000) Chhotanagpur gneiss-granulite complex, Eastern India – A kaleidoscope of global events. *In*: A.N. Trivedi, B.C. Sarkar, N.C. Ghose and Y.R. Dhar (Eds.), Geology and Mineral Resources of Bihar and Jharkhand, Platinum Jubilee Commemorative Volume, Indian School of Mines, Dhanbad, Inst. Geoexpl. Environ. Monograph 2, Patna, pp.33-58.

Ghose, N.C., Simakin, B.M. and Smirnov, V.N. (1973) Some geochronolgical observations on the Precambrians of Chhotanagpur, Bihar, India. Geol. Mag., v.110, pp.481-484.

Green, T.H. (1994) Experimental studies of trace-element partitioning applicable to igneous petrogenesis - Sedona 16 years later. Chem. Geol., v.117, pp.1-36.

Grove, T.L., Kinzler, R.J. and Brown, W.B. (1992) Fractionation of mid-ocean ridge basalt (MORB), *In:* Mantle Flow and Melt Generation at Mid-Oceanic Ridges. Geophysical Monograph 71, American Geophysical Union, Washington, pp.281-310.

Hofmann, A.W. (1988) Chemical differentiation of the earth: the relationship between mantle, continental crust and oceanic crust. Earth Planet. Sci. Lett., v.90, pp.297-314.

Holland, T. and Blundy, J. (1994) Non-ideal interactions in calcic amphiboles and their bearing on amphibole-plagioclase thermometry. Contrib. Mineral. Petrol., v.116, pp.433-447.

Irvine, T.N. and Baragar, W.R.A. (1971) A guide to the chemical classification of common volcanic rocks. Canad. Jour. Earth Sci., v.8, pp.523-548.

Kent, R.W., Saunders, A.D., Kempton, P.D. and Ghose, N.C. (1997) Rajmahal basalt, Eastern India: Mantle sources and melt distribution at a volcanic rifted margin. *In*: J.J. Mahoney and M.F. Coffin (Eds.), Large Igneous Province: Continental, Oceanic and Planetary Flood Volcanism, Geophysical Monograph 100, American Geophysical Union, Washington, pp.145-182.

Lindsley, D.H. (1983) Pyroxene thermometry. Am. Min., v.68, pp.477-493.

Mahadevan, T.M. (2002) Geology of Bihar and Jharkhand. Geological Society of India, 563p.

McDonough, W.F. and Sun, S.S. (1995). The composition of the Earth. *In:* W. F. McDonough, N. T. Arndt and S. Shirey (Eds.), Chemical Evolution of the Mantle, Chem. Geol., v.120, pp.223-253.

Mezger, K. and Cosca, M.A. (1999) The thermal history of the dating of metamorphic and magmatic minerals : implications of the SWEAT correlation. Precambrian Res., v.94, pp.251-271.

Mukherjee, D. (1993) Final report on the integrated study of the anorthosite and associated rocks of Bankura district, West Bengal. Unpubl. Progress Report for Field Session 1987-88 and 1988-89, Geol. Surv. India, Kolkata, 47p.

Mukherjee, D. (1995) Geochemical and tectonic evolution of Bengal anorthosite. Unpubl. Ph.D. Thesis, Patna University, Patna.

Mukherjee, D. and Ghose, N.C. (1992) Precambrian anorthosite within the Chhotanagpur gneissic complex in eastern Indian shield. Indian Jour. Geol., v.64, pp.143-150.

MUKHERJEE, D. and GHOSE, N.C. (1999) Damodar graben: A centre of contrasting magmatism in the Eastern Indian shield margin. *In*: A. K. Sinha (Ed.), Basement Tectonics, 13, Kluwer Academic Publishers, Netherlands, pp. 179-202.

MUKHOPAD'IYAY, M. (1987) Gravity field and its implication to the origin of the Bengal anorthosite. Jour. Geol. Soc. India, v.29, pp.489-499.

NAJAFI, S.J., COX, K.G. and SUKHESWALA, R.N. (1981) Geology and geochemistry of the basalts flows (Deccan Traps) of the Mahad-Mahableshwar section, India. Mem. Geol. Soc. India, no.3, pp.300-315.

NAQVI, S.M. and ROGERS, J. J. W. (1987) Precambrian Geology of India. Clarendon, Oxford, 223p.

OLIVER, R.L. and FANNING, M. (1997) Antarctica : Precise correlation of Palaeoproterozoic terrains. *In*: C.A. Ricci (Ed.), The Antartica Region : geological evolution and processes. Terra Antarctica Publ., Siena, pp.163-172.

PANDEY, B.K., GUPTA, J.N. and LALL, Y. (1986) Whole rock and mineral Rb-Sr isochron ages for the granites from Bihar mica belt of Hazaribagh, Bihar, India. Indian Jour. Earth Sciences, v.12, pp.157-162.

PEARCE, T.H. (1980) Geochemical evidence for the genesis of and eruptive settings of lavas from Tethyan ophiolites. Proc. Intern. Ophiolite Symp., Cyprus, pp.261-272.

PEARCE, J.A. and CANN, J.R. (1973) Tectonic setting of basic volcanic rocks determined using trace element analysis. Earth Planet. Sci. Lett., v.19, pp.290-300.

PELICAT, J.J., MENO, R.P., MONNIER, O. and FANNING, C.M. (1999) The Terra Adelie basement in the East Antarctica shield: Geological and isotopic evidence for a major 1.7 Ga thermal event; comparision with Gawler craton in South Australia. Precambrian Res., v.94, pp.205-224.

RAY BARMAN, T., BISHUI, P.K. and SARKAR, A. (1990) Dating of early Precambrian granite-greenstone complex of the eastern Indian Preacmbrian shield – special reference to Chotanagpur gneissic complex. Rec. Geol. Surv. India, v.123, pt. 2, pp.25-27.

RAY BARMAN, T. and BISHUI, P.K. (1994) Dating of Chhotanagpur gneissic complex of eastern Indian Precambrain shield. Rec. Geol. Surv. India, v.127, pt.2, pp.23-24.

ROEDER, P.L. and EMSLIE, R.F. (1970) Olivine liquid equilibrium. Contrib. Mineral. Petrol., v.29, pp. 275-289.

ROY, K. and SAHA, A.K. (1975) Trace element geochemistry of the Bengal anorthosite and associated rocks. Neus. Jahrb. Mineral Abh., v.125, pp.297-314.

ROY, A., SARKAR, A., JEYAKUMAR, S., AGGRAWAL, S.K. and EBIHARA, M., (2002) Mid-Proterozoic plume-related thermal event in eastern Indian craton : Evidence from trace elements, REE geochemistry and Sr-Nd isotope systematics of basic-ultrabasic intrusives from Dalma volcanics belt. Gondwana Research, v.5, no.1, pp.133-146.

SARKAR, A., GUPTA, S.N., RAY BARMAN, T. and BISHUI, P.K. (1989) Dating of early Precambrian granite-greenstone complex of the eastern Indian Precambrain shield – special reference to Chotanagpur gneissic complex. Rec. Geol. Surv. India, v.122, pt.2, pp.26-27.

SCHILLING, J.G., ZAJAC, M., EVANS, R., JOHNSON, T., WHITE, W., DEVINE, J.D. and KINGSLEY, R. (1983) Petrologic and geochemical variations along the Mid-Atlantic Ridge from 27°N-73°N. Am. Jour. Sci., v.283, pp.510-586.

SENGUPTA, S., PAUL, D.K., BISHUI, P.K., GUPTA, S.N., CHAKRABORTY, R. and SEN, P. (1994) Geochemical and Rb-Sr isotopic study of Kuilapal granite and Arkasani granophyre from the eastern Indian craton. Indian Minerals, v.48, pp.77-88.

SEN, S.K. and BHATTACHARYA, A. (1985) Fluid induced metamorphic changes in the Bengal Anorthosite around Saltora, West Bengal. Indian Jour. Earth Sciences, v.13, no.1, pp.45-64.

SEN, S.K. and BHATTACHARYA, A. (1993) Post-peak pressure-temperature-fluid history of the granulites around Saltora, West Bengal. Proc. Nat. Acad. Sci., v.63(A), pp.280-306.

SEN, S.K. and MANNA, S.S. (1976) Patterns of cation fractionation among pyroxene, hornblende and garnet in the basic granulites of Saltora, West Bengal, India. Indian Jour. Earth Sciences, v.3, pp.117-128.

SHARMA, M., BASU, A.R. and RAY, S.L. (1994) Sm-Nd isotopic and geochemical study of the Archean tonalite-amphibolite association from the eastern Indian craton. Contrib. Miner. Petrol., v.117, pp.45-55.

SUN, S.S. and MCDONOUGH, W.F. (1989) Element concentrations (in ppm) for chondrites, normal enriched-type, mid-ocean ridge basalts (N- and E-MORB), and ocean island basalt (OIB). *In*: A.D. Saunders and A.J. Norry (Eds.), Magmatism in the Ocean Basins, Geol. Soc. Amer. Spec. Publ., no. 42, pp.313-345.

VERMA, R.K., MUKHOPADHYAY, M., ASHRAF, M.H., NAG, A.K. and SATYANARAYANA, Y. (1988) Analysis of gravity field over Chhotanagpur plateau and Bihar mica belt. Mem. Geol. Soc. India, no.8, pp.185-198.

(Received: 28 January 2003; Revised form accepted: 9 February 2005)